Quantifying Receiver Nonlinearities in VNA Measurements for the WR-15 Waveguide Band

Angela C. Stelson, *Member, IEEE*, Aaron M. Hagerstrom, Jeffrey A. Jargon, *Senior Member, IEEE*, and Christian J. Long

***Abstract*— Scattering (*S*)-parameters are fundamental to numerous microwave quantities, including antenna factors, microwave power, and phase. The uncertainty in *S*-parameter measurements is influenced by the test setup, including instrument noise, drift, and position of the cables. In this article, we present a model to assess the uncertainty in *S*-parameter measurements due to nonlinearity in the receivers of a vector network analyzer (VNA). We developed a model that describes the nonlinearity of raw wave parameters and can be propagated through the corrected *S*-parameters. We designed an experiment to extract the parameters of our model for a test setup from measurements of a series of devices under test and demonstrated our model for the WR-15 rectangular waveguide band. This model can correct for or assess uncertainties due to receiver nonlinearity on *S*-parameter measurements and is agnostic to the calibration method used. Using our model, we assess the effects of receiver nonlinearity on calibration error coefficients and the corrected *S*-parameters of one- and two-port devices under test (DUTs).**

***Index Terms*— Calibration techniques, microwave measurements, nonlinear modeling, rectangular waveguide, uncertainty, vector network analysis, waveguide passive devices.**

I. Introduction

IN RECENT years, the telecommunications industry has been working to deploy electronics that operate at millimeter-wave frequencies for 5G networks and beyond. To support the new technologies, advances in microwave metrology are required, including comprehensive, traceable uncertainties on fundamental microwave measurands. Rigorous uncertainty analysis of a scattering (*S*)-parameter measurement on a vector network analyzer (VNA) includes assessment of contributions due to instrument drift, cable positioning, systematic effects due to the calibration artifacts, and receiver nonlinearity [1]. Ideally, such an assessment would include frequency correlations to enable time–frequency domain transformations that are critical to many communications' signal measurements [2].

Large dynamic range is critical to several microwave measurements, including amplifier characterization and load—pull measurements. In these measurements, the receivers can operate in compression and distort the measured *S*-parameters, creating a systematic uncertainty in the measurement. Multiple elements in VNA receivers can be driven into compression at high powers, including amplifiers used to condition the inputs and outputs of the mixer. Because these uncertainty contributions can be difficult to model or remove by calibration, they are often assessed as an uncertainty added to the corrected *S*-parameters after the fact. Strategies to characterize the effects of nonlinearity can rely on precision devices characterized by top-tier calibration laboratories, which can be expensive and hard to maintain [1], [3]. Another major disadvantage of approaches based on precision artifacts is that the nonlinearity is estimated from the deviation of the artifact's measured *S*-parameters from their nominal values as measured by the calibration laboratory. This means that all contributions to the overall uncertainty of the device *S*-parameters increase the uncertainty assessment of the contribution of receiver nonlinearity. Moreover, previous efforts to model nonlinearity contributions to the error box coefficients have found that the contribution depends strongly on the calibration type and the artifacts themselves [4].

Here, we propose a simple, general model for receiver nonlinearity and an experimental method to calculate the coefficients associated with the model. We assess the receiver nonlinearity perturbation directly from measurements of the raw wave-parameter measurements, in contrast to previous methods. This approach makes our model insensitive to the calibration artifacts or calibration type.

We test our approach on measurements in the WR-15 waveguide band, where we demonstrate that our model can correct for the effects of nonlinearity in the error box coefficients as well as corrected *S*-parameters of devices under test (DUTs). We also introduce a scheme for using the model as an uncertainty mechanism and propagate the uncertainties from the raw wave parameters through the corrected *S*-parameters of several DUTs using the National Institute of Standards and Technology (NIST) Microwave Uncertainty Framework [5].[1] Our model and measurement can be easily extended to measurements in other form factors, including coaxial and on-chip measurements.

II. Model

The flow diagram in Fig. 1 illustrates the error model we use to describe the effects of receiver nonlinearity. Here, we use the eight-term error box model with coefficients

Manuscript received October 10, 2021; revised January 10, 2022; accepted February 16, 2022. Date of publication March 15, 2022; date of current version May 5, 2022. *(Angela C. Stelson and Aaron M. Hagerstrom are co-first authors.) (Corresponding author: Angela C. Stelson.)*

The authors are with the National Institute of Standards and Technology, Boulder, CO 80305 USA (e-mail: angela.stelson@nist.gov).

Color versions of one or more figures in this article are available at https://doi.org/10.1109/TMTT.2022.3155466.

Digital Object Identifier 10.1109/TMTT.2022.3155466

[1] In this article, "raw" wave parameters and *S*-parameters have not been corrected by a calibration such as multiline TRL or SOLR. We use "corrected" and "uncorrected" to indicate whether the nonlinearity of the receivers has been accounted for using the techniques we describe here.

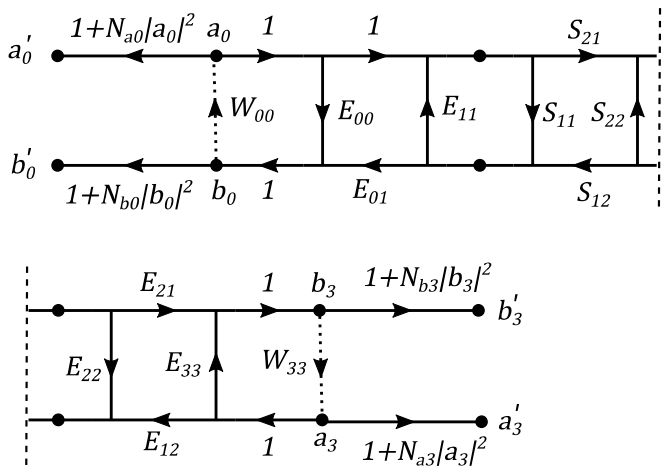

Fig. 1. Flow diagram illustrating the switch-term corrected eight-term error model used in this analysis. The error box model relates the raw wave parameters perturbed by nonlinearity a_i' and b_i' to the corrected S-parameters S_{ij}. The raw unperturbed wave parameters a_i are perturbed by the nonlinearity with coefficients N_{ij}. The eight-term error box components are labeled E_{ij} and the switch terms are labeled W_{ii}.

E_{ij} [6] and switch term corrections W_{ii} [7] to relate raw wave parameters a_i and b_i to the corrected S-parameters S_{ij}. In this report, we will use both multiline thru-reflect-line (TRL) and short-open-load-reciprocal (SOLR) calibrations to determine the error box coefficients, and we report all error coefficients in terms of the model presented in Fig. 1. It is worth noting that the nonlinearity model developed here is quite general and extends to other error models and configurations of VNA that rely on the same receivers.

We model the nonlinearity as a perturbation of the a- and b-waves. We restrict our attention to the case where the stimulus signal has only a single frequency and focus on the effect of the receiver nonlinearity at the stimulus frequency as opposed to higher harmonics. We attribute the perturbation of the measured wave parameters by the nonlinearity of each receiver to a separate coefficient. The relationship between the unperturbed "true" wave parameters and those perturbed by nonlinearity is

$$a_0' = a_0 + N_{a0}|a_0|^2 a_0 \tag{1}$$

$$b_0' = b_0 + N_{b0}|b_0|^2 b_0 \tag{2}$$

$$a_3' = a_3 + N_{a3}|a_3|^2 a_3 \tag{3}$$

and

$$b_3' = b_3 + N_{b3}|b_3|^2 b_3 \tag{4}$$

where, for example, a_n is the true wave parameter and a_n' is the measured wave parameter perturbed by nonlinearity. The perturbed uncorrected S-parameters can be calculated

$$S_{nm}' = \frac{b_n + N_{bn}|b_n|^2 b_n}{a_m + N_{am}|a_m|^2 a_m}. \tag{5}$$

For a series of measurements taken at different power levels j, we denote the measurement with a superscript. Experimentally, we have access to the measured data $a_n^{(j)}$, $b_n^{(j)}$, and $S_{nm}^{(j)}$, while (1)–(4) describe the nonlinear distortion in terms of the true wave parameters. Thus, to facilitate our analysis, we make the approximation $|a_n|^2 \cong |a_n'|^2$ and $|b_n|^2 \cong |b_n'|^2$ and

$$S_{nm}^{(j)} = S_{nm}\left(\frac{1 + N_{bn}\left|b_n^{(j)}\right|^2}{1 + N_{am}\left|a_m^{(j)}\right|^2}\right). \tag{6}$$

Equation (6) still has one true, as opposed to measured, variable, S_{nm}. To derive a relationship between the nonlinearity coefficients and measured S- and wave parameters, we take the ratio of two measurements at different power levels

$$\frac{S_{nm}^{(1)}}{S_{nm}^{(2)}} = \left(\frac{1 + N_{bn}\left|b_n^{(1)}\right|^2}{1 + N_{am}\left|a_m^{(1)}\right|^2}\right)\left(\frac{1 + N_{am}\left|a_m^{(2)}\right|^2}{1 + N_{bn}\left|b_n^{(2)}\right|^2}\right). \tag{7}$$

We take the first term of a Taylor series expansion of the ratios with respect to $N_{am}|a_m^{(1)}|^2$ and $N_{bn}|b_n^{(2)}|^2$ to yield

$$\frac{S_{nm}^{(1)}}{S_{nm}^{(2)}} = \left(1 + N_{bn}\left|b_n^{(1)}\right|^2\right)\left(1 - N_{am}\left|a_m^{(1)}\right|^2\right) \times\left(1 + N_{am}\left|a_m^{(2)}\right|^2\right)\left(1 - N_{bn}\left|b_n^{(2)}\right|^2\right). \tag{8}$$

Finally, we eliminate terms that are higher order than $N_{am}|a_m^{(1)}|^2$ and $N_{bn}|b_n^{(2)}|^2$. The result is a model that relates measurements of raw S-parameters and raw wave parameters to the nonlinear coefficients of our model

$$\frac{S_{nm}^{(1)}}{S_{nm}^{(2)}} - 1 = N_{bn}\left(\left|b_n^{(1)}\right|^2 - \left|b_n^{(2)}\right|^2\right) - N_{am}\left(\left|a_m^{(1)}\right|^2 - \left|a_m^{(2)}\right|^2\right). \tag{9}$$

Note that it is possible to measure the nonlinear coefficients without any knowledge of the S-parameters of the DUT. Also, note that, for the purpose of correcting for the nonlinear distortion, it is not necessary to determine the power incident on the receivers in physical units. The raw values suffice. To correct for nonlinear distortion, we use (1)–(4). For example, a_0^{corr}, our estimate of the true value of a_0 based on the measured value a_0' is given by

$$a_0^{\text{corr}} = a_0' - N_{a0}\left|a_0'\right|^2 a_0'. \tag{10}$$

Similar expressions exist for the other four wave parameters.

III. Measurement Methods

In this section, we use the nonlinear model described in Section II to characterize the effect of receiver nonlinearity for a measurement configuration with extender heads in the WR-15 rectangular waveguide band. To control the power level, we used manual attenuators built into the extender heads. These attenuators are applied to the RF input signal before the signal passes through the couplers and attenuates both the a- and b-waves for each measurement [8]. This is advantageous because our characterization is insensitive to the S-parameters of the attenuator itself, a drawback of other nonlinearity characterization techniques [1]. The power range used to evaluate the nonlinearity was approximately -10 to 10 dBm.

The form of (9) hints at the optimal choice of calibration standards to characterize the nonlinear coefficients of our model. Calibration artifacts that produce a relatively small b-wave make the contribution of the first term on the right-hand side of (9) small, isolating the nonlinear contribution of the a-wave receiver. However, the b-wave must still be large enough that the S-parameter ratio on the left-hand side of the equation is not substantially affected by the noise floor of the VNA, even at the lowest source power levels. For a typical VNA with a dynamic range above 110 dB, a load or attenuator with reflection coefficients around -30 to -60 dB is good candidate for characterizing a-wave nonlinearity. With the a-wave nonlinearity well-conditioned by the measurement of a lossy standard, an additional standard that produces relatively large b-waves (e.g., a short or a thru connection) then serves to provide a well-conditioned equation for nonlinear contribution of the b-wave receiver. We mention again that the S-parameters of these standards do not need to be known explicitly, though any devices chosen to characterize receiver nonlinearity should be highly linear.

We performed a series of raw wave-parameter measurements on four DUTs: a short, load, 30-dB attenuator, and flush thru. For each DUT, we connected the device and measured the raw wave parameters as a function of attenuation. A single connect cycle was used for each DUT to minimize the effects of connection repeatability. Approximately, the same level of attenuation was applied on both ports for each of the measurements, and control measurements of varied attenuation across ports 1 and 2 yielded similar results. The raw S-parameters we present are calculated from the raw wave-parameter data and are not switch-term corrected.

To calculate the nonlinear coefficients from our model, we fit a linear system of equations across the DUTs. Specifically, we simultaneously fit the real and imaginary components of S_{11} and S_{22} of the short and load and S_{21} and S_{12} of the flush thru and the attenuator to the model in (10). The result was an overdetermined fit of the real and imaginary parts of N_{a0}, N_{b0}, N_{a3}, and N_{b3} at each frequency point (50–75 GHz on a 50-MHz grid). This allowed us to evaluate the phase and amplitude nonlinearities of each physical receiver independently.

IV. Results

We observe good agreement between our measurements and the model (Fig. 2). In Fig. 2, the zeroth measurement is the measurement taken at the highest power level, and negative values indicate the compression of the S-parameter as a function of power. Our model is characterized by competing contributions from compression in the a-waves and b-waves (the green lines and orange lines, respectively). For the short and the thru, the b-wave term dominates, resulting in a net compression. However, for the attenuator and the load [Fig. 1(c) and (d)], the nonlinearity effects are dominated by the a-wave receivers, and we see a systematic increase in the S-parameters as a function of power. This trend is consistent with our expectation that a-wave and b-wave receiver compression are both important at high

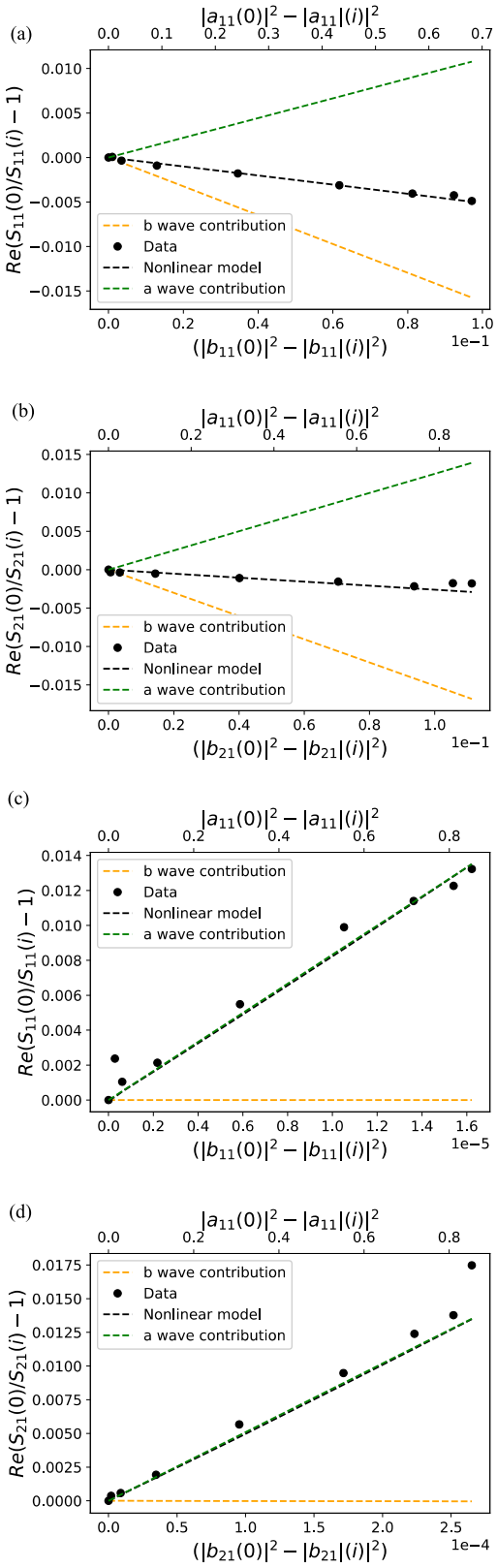

Fig. 2. Nonlinearity model and data. Relative S-parameters for (a) short, (b) flush thru, (c) load, and (d) 30-dB attenuator as a function of wave-parameter amplitude at 50 GHz. Dotted lines are the model and points are measured data. The full nonlinear model is the sum of the a-wave contribution and b-wave contributions. We used the raw wave parameters as reported by the VNA, with arbitrary units. Here, the wave parameters are measured in V.

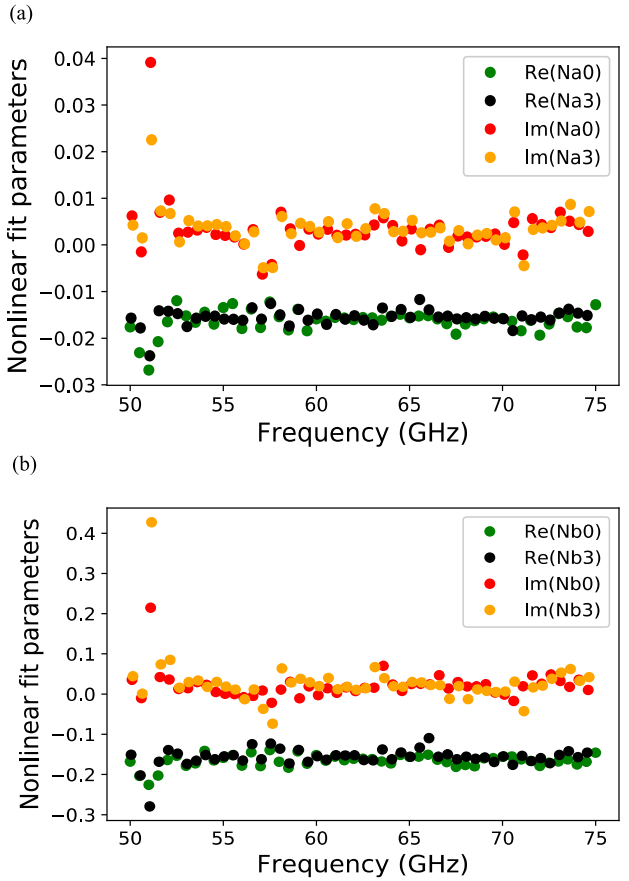

Fig. 3. Nonlinear coefficients for (a) a-wave receivers and (b) b-wave receivers. Each frequency point was calculated independently as a nonlinear fit.

powers and that b-wave receiver compression is relatively unimportant for the small b-waves associated with the load and the attenuator. We also note that directly assessing the nonlinearity on the S-parameters or attributing nonlinearity only to compression in the b-wave receivers would not account for these effects. The largest deviation from our model is observed in the load, where other contributions to uncertainty in the S-parameters (e.g., drift and cable positioning) become a proportionally greater contribution to the small-magnitude wave parameters [9].

The nonlinear coefficients we calculate from our fitting procedure are generally frequency independent and similar across both ports (Fig. 3). The nonlinear coefficients of the a-wave receivers are approximately one order of magnitude lower than the b-wave receiver coefficients. However, because the a-waves have a larger amplitude, the relative magnitude of the a-wave contributions to the nonlinearity can sometimes be the dominant contribution to the nonlinearity in well-matched devices and attenuators, as shown in Fig. 2. Though we allowed for complex nonlinear coefficients in our fitting procedure, we found that across the average imaginary, the nonlinear coefficient was close to zero for all receivers. For a narrow range of frequencies from 51 to 52 GHz, we find that our fit is ill-conditioned for the load and attenuator devices, which helps determine the contribution from the a-wave receiver. Better fits across all frequencies could be achieved by overdetermining the fit with a variety of attenuators. We calculate the nonlinearity coefficients directly from the uncorrected wave parameters of the VNA, and thus, we report the nonlinearity coefficients as arbitrary units relative to the definitions of the VNA. We discard the imaginary component of the nonlinearity coefficient in our uncertainty analysis as the variance is small and centered at zero. Physically, this corresponds to gain compression in the receivers being the dominant source of nonlinearity. We calculate the average nonlinear coefficient of the receivers across all the frequency points to be $N_{a0} = -1.583 \times 10^{-2} \pm 5.400 \times 10^{-3}$, $N_{a3} = -1.489 \times 10^{-2} \pm -2.121 \times 10^{-3}$, $N_{b0} = -0.162 \pm 3.065 \times 10^{-2}$, and $N_{b3} = -0.151 \pm 3.636 \times 10^{-2}$, where the uncertainty is reported as one standard deviation of the measurements taken at all the frequency points. We used the average values reported here to calculate the corrections due to nonlinearity in Figs. 4–6.

To further test our model, we performed a one-port short-open-load (SOL) calibration where we varied the power levels on individual calibration standards. Specifically, we performed a series of calibrations where two standards were measured at approximately -10 dBm and the third was measured at approximately 10 dBm (high power). For each calibration, we calculated the directivity, reflection tracking term, and source match (Fig. 4). For the directivity [Fig. 4(a)], there is a small deviation when the load is measured at higher power than our model corrects for. The reflection tracking [Fig. 4(b)] is perturbed by higher power measurements of reflect standards, and applying the nonlinearity correction to the calibration standards both reduces the noise and corrects the systematic lower values in the reflection tracking. The source match term [Fig. 4(c)] is not clearly affected by standards measured at different power levels. The source match in this measurement configuration was small (less than 0.1), and other studies of receiver nonlinearity suggest that this term would be more dependent on power levels in a test setup with a larger source match term [4]. An additional source of power dependence in the error box coefficients is internal leakages in the VNA, which are not accounted for in this model. Overall, we observe that our model allows us to correct for the nonlinearity in the receivers and yields the same error box coefficients as standards calibrated at power levels where the receiver is not compressed.

Applying the nonlinearity correction directly to the uncorrected wave parameters of the calibration artifacts has two key advantages over a model applied to the error coefficients. The first advantage is that our model is calibration-independent and can be applied in the same way to different calibration types without reassessing the nonlinearity coefficients. The second key advantage is that this approach can predict the deviations of the error box coefficients for calibrations where the standards are perturbed differently due to nonlinearity. Being able to account for varying compression across calibration standards is particularly important for calibrations such as multiline TRL, where the different lengths of line will have different compression in the receivers.

We assessed the contributions due to nonlinearity for a range of DUTs [flush short (Fig. 5) and 30-dB attenuator

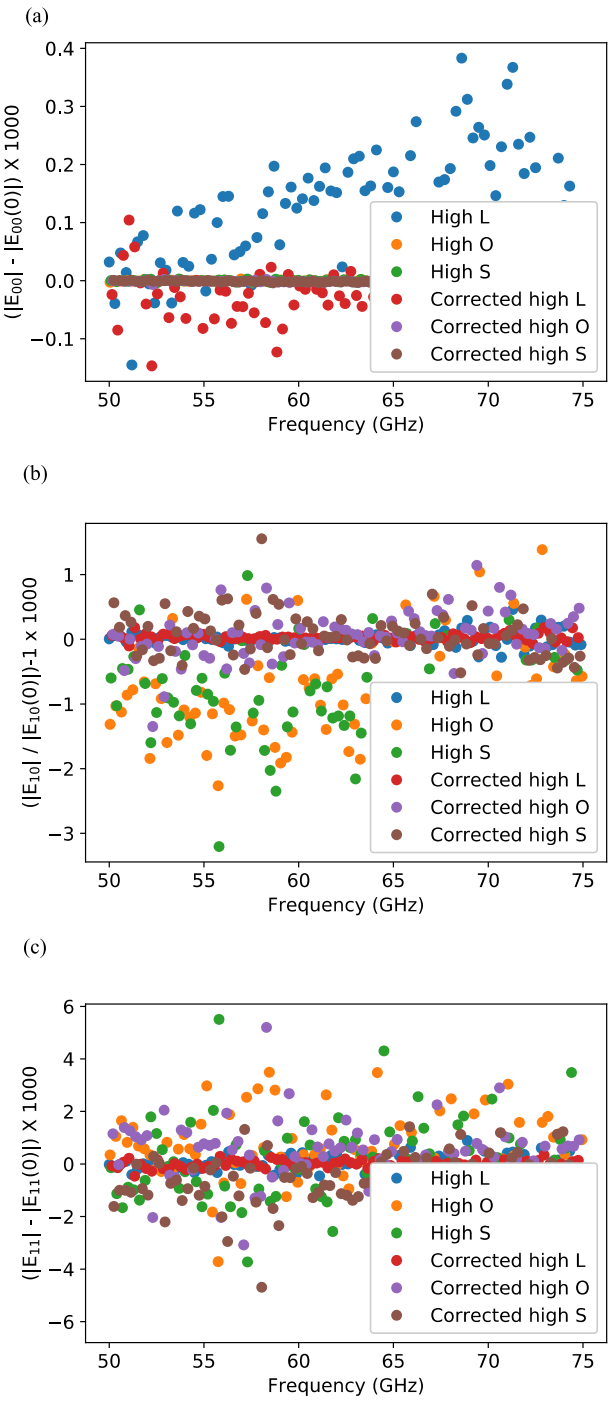

Fig. 4. Normalized change in error box coefficients: (a) E_{00} (directivity), (b) E_{10} (reflection tracking), and (c) E_{11} (source match) for calibrations with calibration standards measured at mismatched high-power levels.

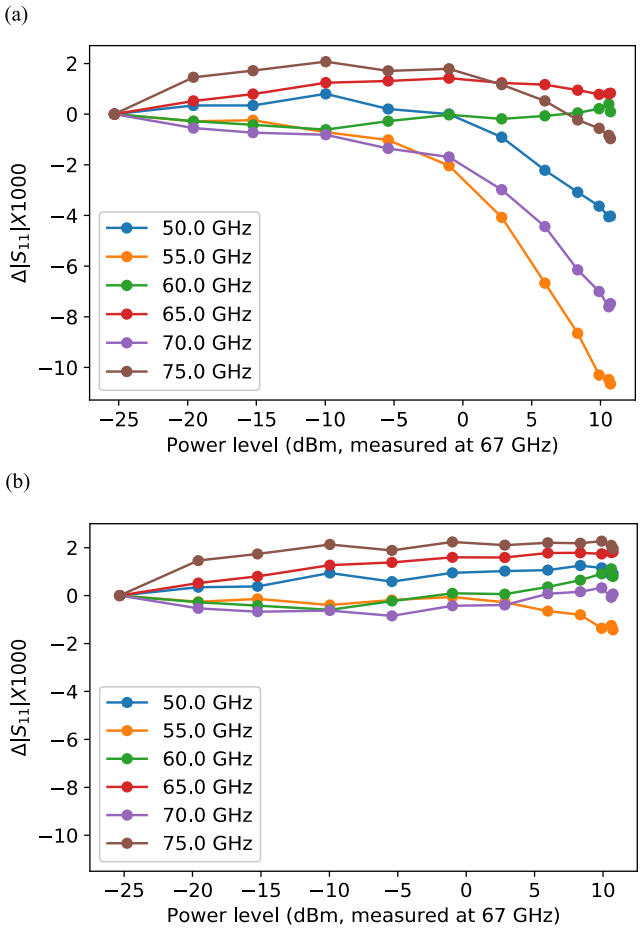

Fig. 5. Calibrated S_{11} of a flush short that is (a) uncorrected for nonlinearity and (b) corrected with the model we present here. The S-parameters are normalized to the measurements taken at −25 dBm.

(Fig. 6)] that were calibrated with multiline TRL using an NIST-traceable kit described in detail elsewhere [10]. We performed these measurements under our typical measurement conditions for passive devices. To minimize the presence of uncertainty mechanisms due to connection cycles, we connected each artifact once and measured it at varying power levels. We then applied our nonlinear correction to the calibration artifact and DUT raw wave parameters and corrected the perturbed S-parameters. When the nonlinear correction is applied, the S-parameters collapse to the value taken at lower power, where the receivers are not in compression [Figs. 5(b) and 6(b)].

We found that nonlinearity was a significant contributor to the uncertainty in $|S_{11}|$ for reflective devices and $|S_{21}|$ of transmissive devices when the devices were measured at power levels above approximately 0 dBm. Under ideal operating conditions where the power levels across all receivers and all standards are comparable and the receivers are not operated in compression, nonlinearity is a minor contributor to the overall uncertainty for the S-parameters. However, under less ideal measurement conditions where the compression asymmetry is large or the calibration and DUT measurement were performed at different levels of compression, nonlinearity can become the dominant contributor to the uncertainty in the magnitude of S-parameters. Compression asymmetry in the receivers can occur in load—pull and amplifier measurements, as well as measurements with high-loss devices.

In addition to correcting for the nonlinearity in our nominal S-parameters, we assess the uncertainty in our model and propagate these uncertainties to the corrected S-parameters of the DUTs. Our uncertainty analysis considers correlations

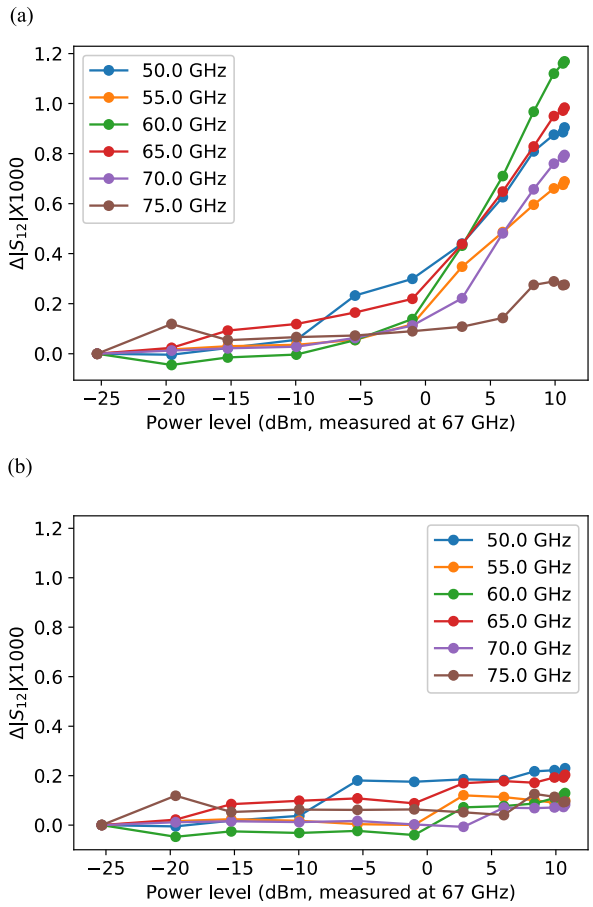

Fig. 6. Calibrated S_{12} of a 30-dB attenuator that is (a) uncorrected for nonlinearity and (b) corrected with the model we present here. The S-parameters are normalized to the measurements taken at −25 dBm.

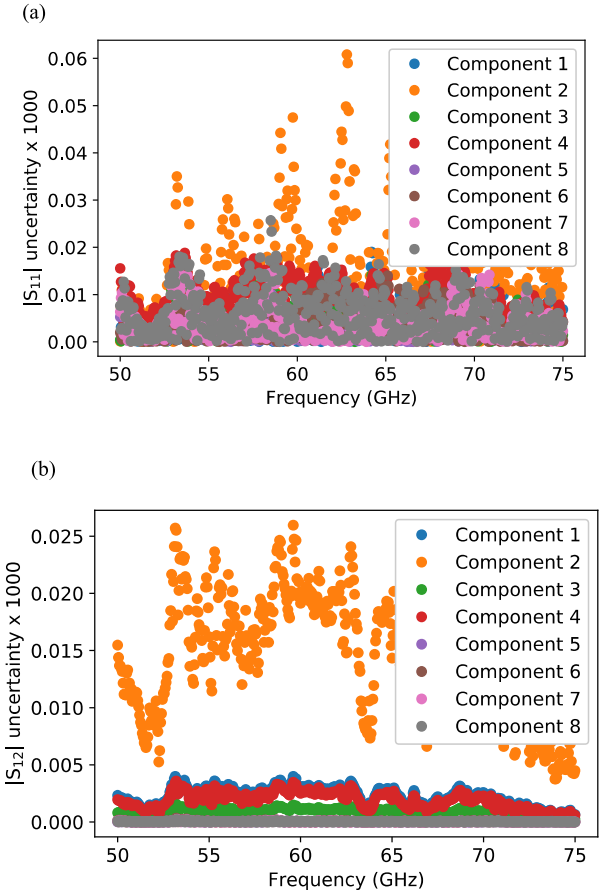

Fig. 7. Standard uncertainty contributions of the principal components of the nonlinear coefficients propagated to (a) S_{11} of a flush short and (b) S_{12} of a 30-dB attenuator. The data were corrected with a multiline TRL calibration. Components are ranked according to their contributions to the variance of complex N.

in the measurement errors of the four nonlinear coefficients. We performed a principal components analysis and treated each frequency point as a sample of the 8-D real vector formed from the real and imaginary parts of the four nonlinear coefficients. We determined the sample covariance matrix and calculated the eigenvectors and eigenvalues. We normalized the eigenvectors so that their squared magnitude is equal to their associated eigenvalue (variance). In our sensitivity analysis, we treated each of these eigenvectors as an uncertainty mechanism. Specifically, we perturbed the raw wave parameters of the calibration artifacts and DUTs by the uncertainty in the nonlinearity contribution given by these eigenvectors. For each uncertainty mechanism, we then propagated these changes to our final measurement result and considered the difference between the perturbed values and our nominal values as the standard uncertainty ($k = 1$) associated with that mechanism. To perform this calculation, we used the NIST Microwave Uncertainty Framework, which handles uncertainty-mechanism propagation for common calibrations including SOL-Thru (SOLT) and multiline TRL [5].

The uncertainty in our nonlinearity model is a small contributor to the overall uncertainty in the S-parameters of a DUT (Fig. 7). Comprehensive assessments of uncertainty contributions in WR-15 typically lead to uncertainties in the range of 1% for $|S_{11}|$, and the uncertainty contributions from our nonlinearity model are several orders of magnitude smaller. [11] It is important to note that here, we assess the uncertainty in our model, not the perturbation due to nonlinearity itself. If the DUT is measured at a much higher power level than the calibration standards, the perturbation due to nonlinearity can be a leading contribution to uncertainty in the S-parameters (see Fig. 5, where the deviation can be on the order of 1%). Here, we propose to apply a correction to the S-parameters to account for nonlinearity and assess uncertainties on that correction.

V. Conclusion

In this report, we developed a model to describe the contributions in receiver nonlinearity in S-parameter measurements. Our model was able to correct for perturbations due to nonlinearity in S-parameters and error box coefficients. We also demonstrated the application of this model as an uncertainty mechanism in a traceable multiline TRL calibration and found that under ideal operating conditions, nonlinearity is a minor contributor to the overall uncertainty but becomes increasingly important when devices are lossy or measured at variable compression levels. The model we develop and our method for assessing nonlinearity is generalizable to other calibrations and connector types. Looking forward, this model can be applied

to correct for or assess uncertainty due to receiver nonlinearity in more complex measurement setups, including on-chip measurements with lossy materials, large signal network analyzer (LSNA) measurements, and load—pull measurements.

A. Experimental Methods

We performed all measurements on a Rhode and Schwarz ZVA 67 four-port VNA in combination with Virginia Diodes, Inc. (VDI) WR-15 extender heads. We used an intermediate-frequency bandwidth (IFBW) of 10 Hz and an average factor of 1 for all measurements. The VNA and extender head setup was designed to minimize stress on the cables attached to the extender heads, with the extender heads placed level with the VNA ports. All measurements were performed on the same test ports that were dimensionally characterized to be within 0.0035 mm of the ideal WR-15 dimensions. The calibration artifacts and DUTs were measured at 501 frequency points, spaced linearly from 50 to 75 GHz. All one-port measurements were performed with DUTs attached to both ports to prevent crosstalk, and equivalent DUTs were measured simultaneously on each port. For the measurements performed at our standard operating conditions, we use a power level calibrated at −10 dBm at 67 GHz.

ACKNOWLEDGMENT

The authors would like to thank D. F. Williams, National Institute of Standards and Technology (NIST), Boulder, CO, USA, and P. D. Hale, Z. Fishman, N. Jungwirth, and J. C. Booth, NIST, for their critical review of this article and valuable contributions to this work.

Certain commercial equipment, instruments, or materials are identified in this article in order to specify the experimental procedure adequately. Such identification is not intended to imply recommendation or endorsement by the National Institute of Standards and Technology nor is it intended to imply that the materials or equipment identified are necessarily the best available for the purpose.

REFERENCES

[1] M. Zeier, D. Allal, and R. Judaschke, "Guidelines on the evaluation of vector network analyzers (VNA)," Eur. Assoc. Nat. Metrol. Inst., Brunswick, Germany, Tech. Rep. Calibration Guide 12, 2018, vol. 3.

[2] D. F. Williams, B. Jamroz, and J. D. Rezac, "Evaluating uncertainty of nonlinear microwave calibration models with regression residuals," *IEEE Trans. Microw. Theory Techn.*, vol. 68, no. 9, pp. 3776–3782, Sep. 2020, doi: 10.1109/TMTT.2020.3005170.

[3] K. Wong, "VNA receiver dynamic accuracy specifications and uncertainties—A top level overview," Keysight Technol., USA, Tech. Rep. Reference Guide N5247-90104, 2010.

[4] J. Martens, "On quantifying the effects of receiver linearity on VNA calibrations," in *Proc. 70th ARFTG Microw. Meas. Conf. (ARFTG)*, Nov. 2007, pp. 1–6, doi: 10.1109/ARFTG.2007.8376223.

[5] D. Williams, B. Jamroz, and A. Lewandowski, *NIST Microwave Uncertainty Framework (Beta version)*. Gaithersburg, MD, USA: NIST, 2021.

[6] D. C. DeGroot, J. A. Jargon, and R. B. Marks, "Multiline TRL revealed," in *60th ARFTG Conf. Dig.*, 2002, pp. 131–155, doi: 10.1109/ARFTGF.2002.1218696.

[7] R. B. Marks, "Formulations of the basic vector network analyzer error model including switch-terms," in *50th ARFTG Conf. Dig.*, vol. 32, Dec. 1997, pp. 115–126, doi: 10.1109/ARFTG.1997.327265.

[8] J. Hesler, J. L. Hesler, Y. Duan, B. Foley, and T. W. Crowe. (2010). *THz Vector Network Analyzer Measurements and Calibration Tunable THz Antenna View Project Variable mm-Wave Attenuator View Project THz Vector Network Analyzer Measurements and Calibration*. [Online]. Available: https://www.researchgate.net/publication/229036688

[9] *Vector Network Analyzer Uncertainty Calculator*, Keysight Technologies, Santa Rosa, CA, USA, 2021.

[10] J. A. Jargon *et al.*, "Physical models and dimensional traceability of WR15 rectangular waveguide standards for determining systematic uncertainties of calibrated scattering-parameters," NIST, Gaithersburg, MD, USA, Tech. Rep. 2109, Aug. 2020, doi: 10.6028/NIST.TN.2109.

[11] T. Schrader, K. Kuhlmann, R. Dickhoff, J. Dittmer, and M. Hiebel, "Verification of scattering parameter measurements in waveguides up to 325 GHz including highly-reflective devices," *Adv. Radio Sci.*, vol. 9, pp. 9–17, Jul. 2011, doi: 10.5194/ars-9-9-2011.

Angela C. Stelson (Member, IEEE) received the B.S. degree in physics, mathematics, and political science from the University of Oregon, Eugene, OR, USA, in 2012, and the Ph.D. degree in materials science and engineering from Cornell University, Ithaca, NY, USA, in 2017. Her graduate work focused on the electric field-directed assembly of colloids for photonic crystals.

She joined the National Institute of Standards and Technology (NIST), Gaithersburg, MD, USA, as a National Research Council Fellow, in 2017. She is currently working with the RF Electronics Group, NIST, developing traceable scattering parameter calibrations and new microwave microfluidics measurement techniques for chemical and biological applications.

Aaron M. Hagerstrom received the B.S. degree in physics from Colorado State University, Fort Collins, CO, USA, in 2010, and the Ph.D. degree in physics from the University of Maryland, College Park, MD, USA, in 2015.

He joined the National Institute of Standards and Technology (NIST), Gaithersburg, MD, USA, in 2016, as an NRC Post-Doctoral Associate, and developed techniques for microwave-frequency characterization of nonlinear materials and devices. In 2019, he was hired into a Staff Position with NIST, to research traceable power measurements at microwave and millimeter-wave frequencies.

Jeffrey A. Jargon (Senior Member, IEEE) received the B.S., M.S., and Ph.D. degrees in electrical engineering from the University of Colorado at Boulder, Boulder, CO, USA, in 1990, 1996, and 2003, respectively.

He has been a Staff Member with the National Institute of Standards and Technology (NIST), Boulder, since 1990, where he has conducted research in the areas of vector network analysis, optical performance monitoring, and waveform metrology. He is currently a member of the High-Speed Measurements Project with the Communications Technology Laboratory, NIST. He is a registered Professional Engineer in the State of Colorado and an ASQ Certified Quality Engineer.

Dr. Jargon was a recipient of six best paper awards, including the URSI Young Scientist Award and the Department of Commerce Silver Medal Award.

Christian J. Long received the B.S. and Ph.D. degrees in physics from the University of Maryland, College Park, MD, USA, in 2004 and 2011, respectively. His Ph.D. research focused on the development of both microwave near-field scanning probe microscopy techniques and new methods to analyze data from combinatorial materials experiments.

From 2012 to 2015, he was a Post-Doctoral Researcher with the National Institute of Standards and Technology (NIST), Gaithersburg, MD, USA, where he focused on techniques for characterizing nanoscale materials. In 2016, he joined NIST, Boulder, CO, USA, as a Staff, where he currently leads the Microwave Power and Impedance Project.